Development of the Multifrequency Gyrotron FU CW GV with Gaussian Beam Output

Yoshinori Tatematsu [1] · **Yuusuke Yamaguchi** [1] ·
Ryoichi Ichioka [1] · **Masaki Kotera** [1] · **Teruo Saito** [1] ·
Toshitaka Idehara [1]

Abstract Gyrotron FU CW GV has been developed as a multifrequency gyrotron for operation over the frequency range from 162 to 265 GHz at frequencies separated by steps of approximately 10 GHz. The oscillation modes were selected; the radii of the caustic surfaces for the electromagnetic waves of the modes had similar values in the waveguide, and it was therefore expected that these modes would be converted into Gaussian beams by a mode converter. In reality, more than ten modes oscillated and the Gaussian-like beams were radiated. A double-disk window with variable spacing maintains the transmittance through the window at a high level over a wide range of frequencies. Using this window, output powers of more than 1 kW were observed for almost all the expected modes.

Keywords Gyrotron · Multifrequency operation · Gaussian beam · Mode converter · Double-disk window · High-power radiation source

1 Introduction

At the Research Center for Development of Far-Infrared Region, University of Fukui, Japan (FIR UF), a number of high-frequency gyrotrons operating at frequencies in ranges from sub-THz to THz, including those of the Gyrotron FU-series, the Gyrotron FU CW-series, and the Gyrotron FU CW G-series, have been developed [1–9]. The gyrotrons of the FU CW G-series are equipped with an internal mode converter that converts the electromagnetic (EM) wave that is oscillating in the cavity into a Gaussian beam. Applications based on these gyrotrons have begun to be implemented, including sensitivity enhancement of nuclear magnetic resonance (NMR) spectroscopy with the dynamic nuclear polarization (DNP) method

✉ Yoshinori Tatematsu
tatema@fir.u-fukui.ac.jp

[1] Research Center for Development of Far-Infrared Region, University of Fukui, Fukui 910-8507, Japan

[10, 11], measurements of positronium hyperfine splitting [12–14], and ceramic sintering [15, 16]. FIR UF is thus becoming both a domestic and an international center for joint research into the far-infrared region by providing many advanced gyrotrons.

A gyrotron equipped with an internal mode converter is expected to have one or a few oscillation frequencies, because the converter configuration is determined by the oscillation modes. However, if FIR UF is to seek to become a center for joint research, it is preferable that it provides a gyrotron that radiates EM waves at various frequencies. In principle, it is possible that EM waves with various frequencies will oscillate in the gyrotron cavity if the cavity's magnetic field strength is changed appropriately [7, 17–20], and Gaussian-like beams have previously been observed with several cavity oscillation modes in a single gyrotron [7, 19]. Therefore, the new multifrequency Gyrotron FU CW GV was planned. This gyrotron can radiate Gaussian beams for a number of EM waves with the frequency width of 100 GHz.

One serious obstacle to realization of a multifrequency gyrotron is that the window transmittance of the EM wave is closely dependent on the frequency. For some frequencies, the reflectance is so high that the output power is substantially reduced. There are two possible ways to solve this problem and improve the transmittance at all frequencies [21]. The first is to set the window disk obliquely at the Brewster angle (θ_B) against the direction of the wave propagation, at which all p-polarized waves have transmittance of almost unity, independently of their frequencies. However, θ_B can be as large as 72° for the sapphire used as the window material here; the shape of the window then becomes oval with an axial ratio of approximately 3, and the window disk size increases to more than three times the size of a disk normal to the wave propagation direction, and the window port length becomes very long. Also, a difficult sapphire disk cutting process is necessary to avoid double diffraction, and this process may result in deformation of the radiated beam and variation of the polarization. For these reasons, the oblique window at θ_B was not adopted in the Gyrotron FU CW GV.

The other way to solve the problem is to use a double-disk window. By varying the distance between the two disks, the wave transmittance through the window can be changed in the manner of a Fabry-Perot interferometer [22]. Therefore, by selecting a suitable distance for each frequency, the transmittance can be close to unity as long as the absorption is negligible. Therefore, a double-disk window configuration has been adopted.

In this paper, we describe the design consideration for Gyrotron FU CW GV in Sect. 2. The experimental results are given in Sect. 3. Finally, a summary of the work is provided in Sect. 4.

2 Gyrotron FU CW GV

Gyrotron FU CW GV was developed as the fifth gyrotron in the Gyrotron FU CW G-series [5–9]. A photograph of the gyrotron is shown in Fig. 1. The gyrotron is the sealed-off type and was constructed by New Japan Radio Co., Ltd. The gyrotron was installed on a 10 T magnet, which has a room temperature bore diameter of 100 mm. The cavity radius R_{cavity} is 5.50 mm, and the length of the straight section is 15 mm; at the ends of this section, up and down tapers are connected. The oscillation mode that gives the maximum wave frequency is $TE_{10,6}$ at the fundamental cyclotron resonance, at a frequency of 265 GHz. We therefore call the $TE_{10,6}$ mode the main mode. The mode converter consists of a helically cut launcher and four mirrors, similar to that used in the other gyrotrons of the Gyrotron FU CW G-series [5–7]. The cut angle of the helical launcher is related to the propagating EM wave mode. The mode converter was therefore designed for the $TE_{10,6}$ mode in this gyrotron. However, it was expected that

Fig. 1 Photograph of Gyrotron FU CW GV

several modes would oscillate in the cavity and that the EM wave would be converted into a Gaussian beam by the converter. The expected oscillation modes are listed in Table 1, where the frequencies were calculated using the cold cavity model. The angle θ is defined as $\cos^{-1}(m/\chi'_{m,n})$, where $\chi'_{m,n}$ is the n-th zero of the derivative of the m-th order Bessel function, $\dot{J}_m(z)$, and the eigenvalue of the $TE_{m,n}$ mode. The quantity $m/\chi'_{m,n}$ is an important factor that determines the direction and extension of a beam emitted from a Vlasov launcher [7]. In geometrical optics, the radius of the caustic surface of the EM wave is represented by $R_w \cos\theta$ in the waveguide [23, 24], where R_w is the waveguide radius. It is thus expected that modes with θ values that are close to that of the main mode ($TE_{10,6}$) can oscillate in the cavity, will be converted into a Gaussian beam by the same converter, and will be radiated from the window as a Gaussian beam, because their caustic radii have almost identical values. The ten modes listed in Table 1 are therefore selected as the expected oscillation modes.

The calculated radiation patterns of the EM waves launched from the gyrotron window for some of the oscillation modes are shown in Fig. 2. These patterns were calculated using an EM wave code that was developed at FIR UF. The radiation pattern is a projection of a radiated

Table 1 Cavity modes and frequencies expected to oscillate and be converted into Gaussian beams in Gyrotron FU CW GV, where θ, $R_{b,opt}$, and r_m are defined in the text

Mode	Frequency (GHz)	θ (°)	$R_{b,opt}$ (mm)	r_m
$TE_{10,6}$	265.0	70.9	1.93	42.0
$TE_{9,6}$	253.6	72.1	1.81	47.7
$TE_{8,6}$	242.1	73.3	1.69	54.7
$TE_{7,6}$	230.4	74.7	1.55	65.0
$TE_{9,5}$	224.7	69.7	2.05	37.2
$TE_{8,5}$	213.4	71.0	1.91	42.8
$TE_{7,5}$	202.0	72.5	1.77	49.9
$TE_{6,5}$	190.5	74.1	1.61	60.3
$TE_{7,4}$	173.2	69.5	2.07	36.5
$TE_{6,4}$	161.9	71.2	1.89	43.7

beam onto a plane located at a distance L of 757 mm from the gyrotron's center axis. The X and Y axes indicate the horizontal and vertical directions, respectively, and the origin corresponds to the position that extends horizontally from the window center. The direction of the field of view is such that the window is seen from the outside. Figure 2a–d shows the patterns for the $TE_{10,6}$, $TE_{8,6}$, $TE_{9,5}$, and $TE_{6,5}$ cavity modes, respectively. For the $TE_{10,6}$ mode (i.e., the main mode) oscillation, the center of the wave beam is located near the origin. The center positions of the other modes are shifted only from the origin in the horizontal direction [7]. The X-coordinate of the beam center, X_c, is plotted as a function of $m/\chi'_{m,n}$ of the cavity modes in Fig. 3. A monotonic relationship is found, and similar results were obtained in experiments using other gyrotrons [7, 25]. Among the expected modes listed in Table 1, the EM wave beam that was converted from the $TE_{7,6}$ mode is irradiated from the window most obliquely; however, the angle of ejection of the beam relative to the normal direction of the window disk is only 0.6°. The final (fourth) mirror is rotatable and movable, which means that it is possible to adjust the beam direction to be vertical to the window surface for all cavity modes, although the beam center position is not at the window's center. The total power of the EM waves on the calculated plane is somewhat reduced from the total radiated by the launcher because of diffraction losses that occurred during propagation through the mirrors of the mode converter. The power ratios are 0.94, 0.93, 0.93, and 0.92 for Fig. 2a–d, respectively.

A magnetron injection gun (MIG) was designed using the EGUN code [26]. The gun generates high-quality electron beams with only a small velocity spread under conditions of a cathode voltage of −20 kV, a beam current of 0.5 A, and a pitch factor (the orbital-to-axial electron velocity ratio) of 1.3 for all modes listed in Table 1. The MIG is a triode-type gun, and details of the MIG design will be published elsewhere. The optimal incident radius of the electron beam, $R_{b,opt}$, is different and the magnetic compression ratio between the magnetic field strength at the cavity center and that at the cathode, r_m, should be optimized for each oscillation mode. These values are also given in Table 1, where $R_{b,opt}$ is calculated as $(\chi'_{m-1,1}/\chi'_{m,n})R_{cavity}$ for the corotating mode. Adjustment of $R_{b,opt}$ is achieved by tuning the current in the gun coils that are set around the MIG during the actual measurements. All values of $R_{b,opt}$ in Table 1 lie within a range that is tunable via the current of our power supply.
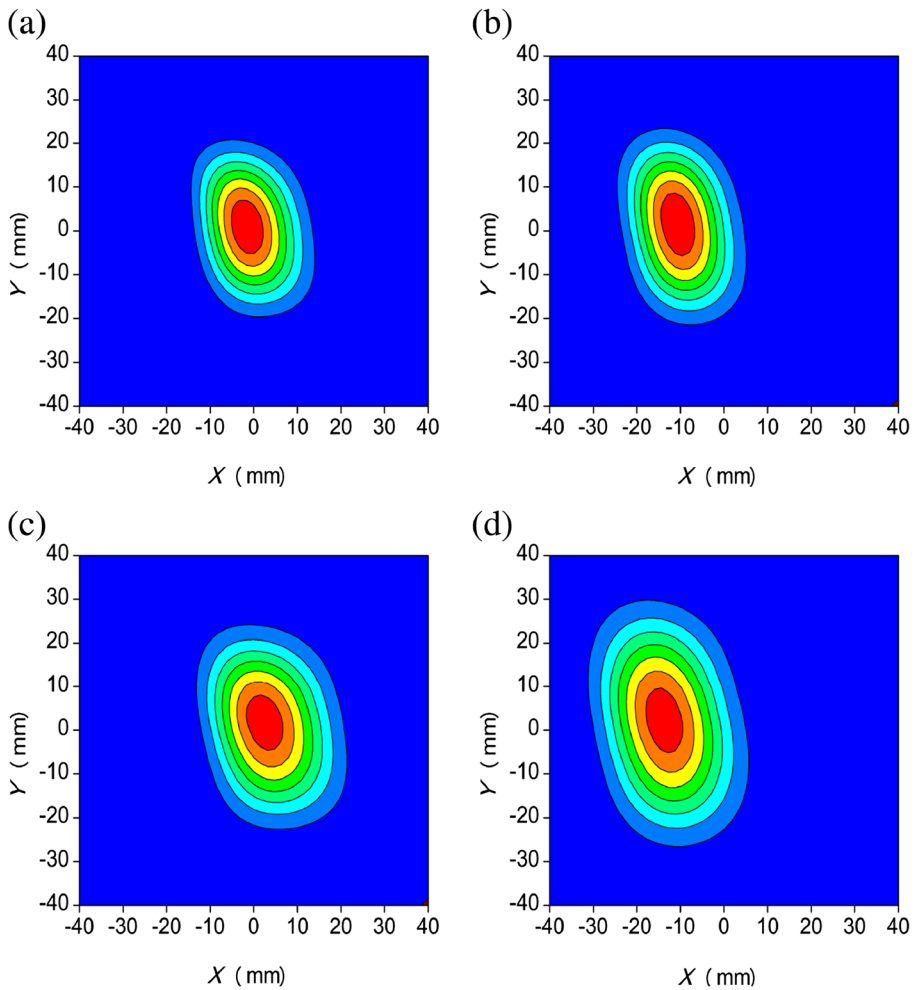
Fig. 2 Calculated radiation patterns for **a** $TE_{10,6}$, **b** $TE_{8,6}$, **c** $TE_{9,5}$, and **d** $TE_{6,5}$ modes at $L=757$ mm

The window disk is made from single crystal sapphire. The disk thickness is 2.946 mm, which was determined such that it allows the main mode to be transmitted without reflection. The power transmittance is calculated via the scattering matrix for different frequencies as shown in Fig. 4. Here, the values that were measured by terahertz-time domain spectroscopy (THz-TDS) at FIR UF were used as the real part of the permittivity of sapphire. However, for the imaginary part of the permittivity, $\tan\delta=2\times10^{-4}$ was assumed based on [27], by extending it to the frequency domain used here, because of the rather low accuracy of the measured value of the imaginary part. The transmittance of the EM wave through the window depends on the wave frequency. The values for the expected modes are represented by the closed circles shown in Fig. 4. While the power absorption rate of the single window disk depends on the frequency, it is less than 1.7 % in the frequency domain used. It is impossible for all EM waves excited within the cavity to be transmitted through the single disk window without reflection, so the output power becomes smaller than the oscillated power value at the cavity exit for
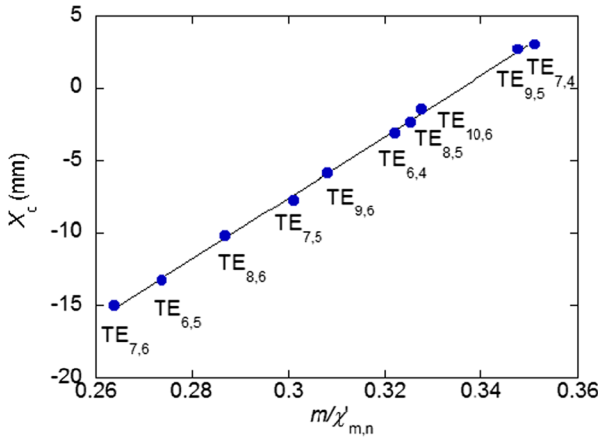
Fig. 3 Calculated beam center positions plotted as a function of $m/\chi'_{m,n}$ at $L=757$ mm

frequencies with low transmittance. To solve this problem, a double-disk window with adjustable disk separation distance was adopted. A schematic view of the window is shown in Fig. 5. The double-disk window was manufactured by the Kyocera Corporation. The second disk was attached to a metal frame, which was then engaged with the main window flange via a screw. The 1-mm pitch screw is cut on the frame. The distance between the two disks was varied from 6 to 11 mm by rotating the frame. The transmittance of the EM wave periodically changed with the variation of the distance between the two disks, d, because of wave interference. The calculated transmittance for $f=224.7$ GHz ($TE_{9,5}$ mode) is shown as an example in Fig. 6. Here, the power transmittance T for this frequency is 0.35 for the single-disk window. If a suitable distance is chosen, T increases up to 0.97, where the assumed permittivity value of sapphire is the same as that used in the calculation for Fig. 4. For all frequencies (modes), the transmittance can be similarly set at almost unity. The main window edge is cooled with water, and the second disk is cooled by thermal conduction through the metal frame of the attached cooled flange of the main window.

Fig. 4 Window power transmittance dependence on wave frequency, where values for the expected oscillation modes are indicated by *closed circles*
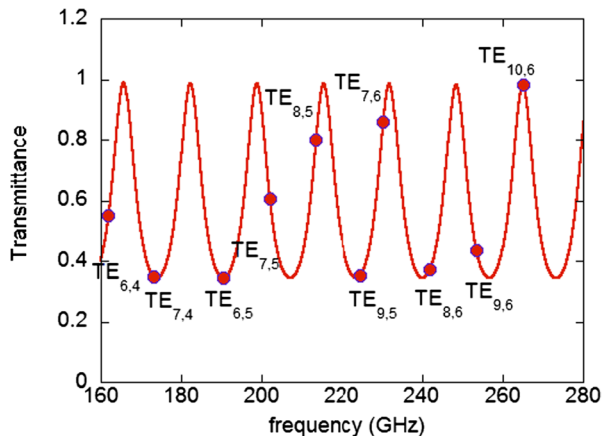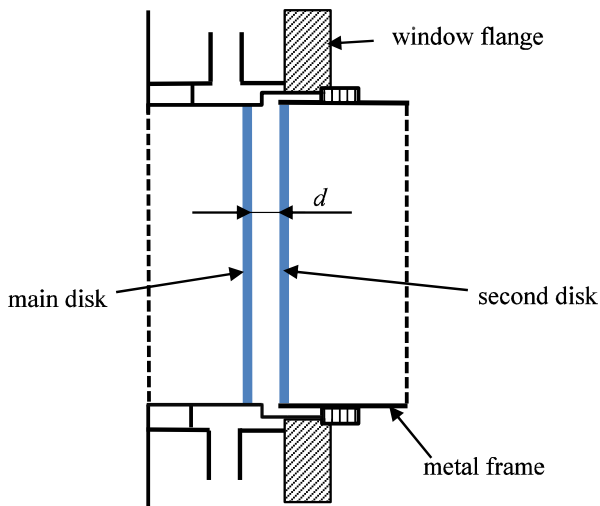
Fig. 5 Schematic view of the double-disk window

The electron beam collector is electrically insulated from the body including the cavity, the waveguides, and the mode converter. The collector and the body are connected to ground via individual resistances. Therefore, the collector current for electrons streaming into the collector can be measured independently of the body current formed by electrons streaming into the body.

3 Experimental Results

The signal intensity of the radiated wave was measured using a pyroelectric detector placed in front of the window while varying the cavity magnetic field strength B. At this stage, the second disk of the window was not attached. The cathode voltage V_K and anode voltage V_A
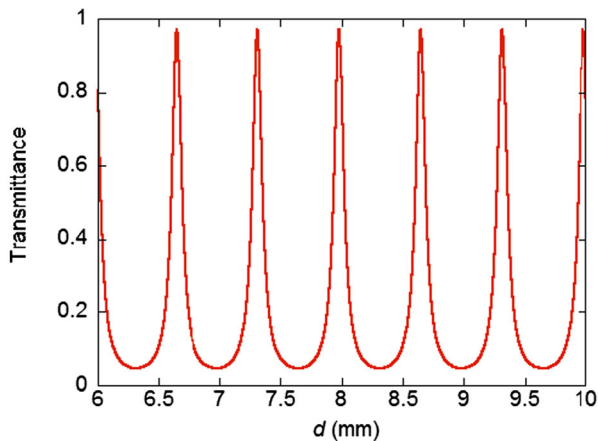

Fig. 6 Calculated power transmittance of double-disk window for f=224.7 GHz

were fixed at −15 and −8 kV, respectively. The magnetic field strength was scanned from 9.8 T to the low B side. The results are shown in Fig. 7, where numerous signal peaks can be observed. The lower side limit of 6.8 T is due to the rapid increase in the body current. The frequency was measured for each peak with a heterodyne receiver system, and the cavity modes were then identified from the measured frequencies. The identified modes and the measured frequencies in GHz are shown in Fig. 7. The measured frequencies agreed well with the calculated values given in Table 1.

Only the signal intensity of the main mode (TE$_{10,6}$) in Fig. 7 is very strong. However, there are some reasons for this behavior. The first is that the measurements were performed with the single-disk window, for which the width has been optimized for the main mode. Another reason is that the incident electron beam radius R_b was not optimized for any modes other than the main mode, because only B was changed. Also, although the beam radiation directions were different for the cavity modes, the detector position was fixed, and the detection area was smaller than the beam cross section. These are the main reasons why the signal intensities of the other modes were much smaller than that of the main mode.

The second disk was then attached to the main window flange. The operating conditions were tuned to enable each expected mode to oscillate with a high output signal. The signal intensity was observed while the distance between the window disks was varied. An example of the results of such a measurement at B=8.208 T, at which TE$_{9,5}$ oscillates, is shown in Fig. 8. The distance d was converted based on the frame rotation angle. The signal was measured at each 1/100th revolution of the frame, i.e., at each 10-μm shift. When d was varied, the measured signal intensity changed periodically. The distance between adjacent peaks corresponds to one half of the wavelength of the radiation wave. From the results shown in Fig. 8, the frequency is estimated to be 225.4 GHz. The difference between the calculated value and the accurately measured value of 224.7 GHz is only 0.7 GHz (0.3 %).

The measurement results in Fig. 8 agree well with the calculated results shown in Fig. 6. If the reflection of the wave from the window influences on the cavity oscillation, then the signal form will deviate from the calculated result. Therefore, the window reflection does not affect the oscillation greatly in the present case. The horizontal dashed line in Fig. 8 indicates the signal intensity level that was obtained using the single-disk window. The transmittance can
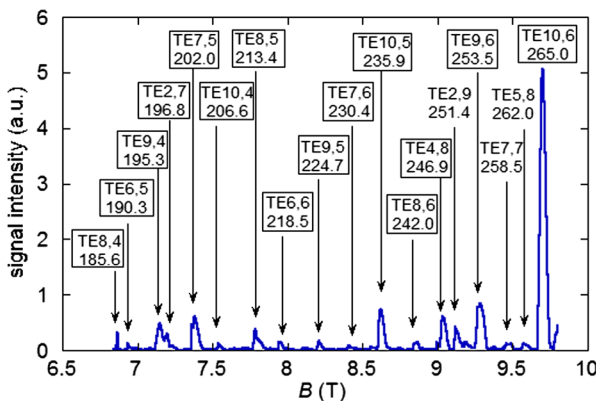
Fig. 7 Signal intensity and frequency measurements on Gyrotron FU CW GV with single-disk window, *the upper and lower letters* indicate the identified modes and the measured frequencies (in GHz), respectively
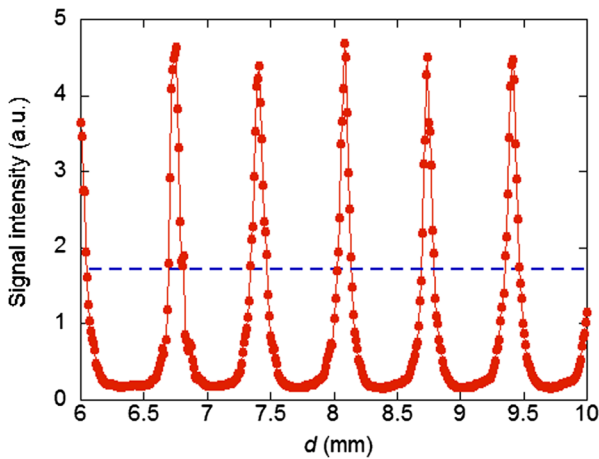
Fig. 8 Measured signal intensity (indicated by *circles*) with double-disk window for f=224.7 GHz, and signal level (*dashed line*) obtained with single-disk window

thus be significantly improved by setting appropriate disk distances for the double-disk window. For the $TE_{7,4}$ and $TE_{6,4}$ modes which oscillate at B of less than 6.8 T, the operating conditions were optimized, and the output signals were observed with small body currents. We thus confirmed the oscillations of all the expected modes in Table 1.

The radiation patterns were then observed for the expected modes using an infrared camera as the temperature increased on a vinyl chloride plate placed in front of the window. The plate was placed parallel to the window surface at a distance of 757 mm from the center axis of the gyrotron tube. Some of these radiation patterns are shown in Fig. 9 and are viewed from the side of the plate opposite that on which the EM wave beam was incident. The cavity modes shown are the $TE_{10,6}$, $TE_{8,6}$, $TE_{9,5}$, and $TE_{6,5}$ modes, respectively. Bi-Gaussian-like beams were observed that were similar to the calculated patterns shown in Fig. 2. In addition to these modes, Gaussian-like patterns were obtained for the other modes. The labels of the oscillation modes for which Gaussian-like beams were radiated from the window are surrounded by squares. Almost all the observed modes were converted into Gaussian-like beams by the same converter.

Next, the window power was measured using a water load for this gyrotron. A cathode voltage of −20 kV and a beam current of 0.5 A were applied. The other operating parameters such as the anode voltage, the magnetic field strength, and the window disk separation distance were optimized for each oscillation. The EM wave power that radiated from the window was gathered by a horn taper with an entrance diameter that was large enough to cover the gyrotron window, and the power that was radiated through the window was absorbed by the water inside a vessel. The results are shown in Fig. 10. Here, the evaluation of the radiation power was achieved under the assumption that the heat capacity of the water vessel and the power loss during the measurement can be neglected, and by assuming that all the power was absorbed by the water load. Therefore, it is reasonable to assume that the actual power radiated from the window was higher than the evaluated power. Open triangles represent the measured power for the single-disk window. The variation of the measured power against the frequency corresponds well with that of the closed circles in Fig. 4. The output power increases with use
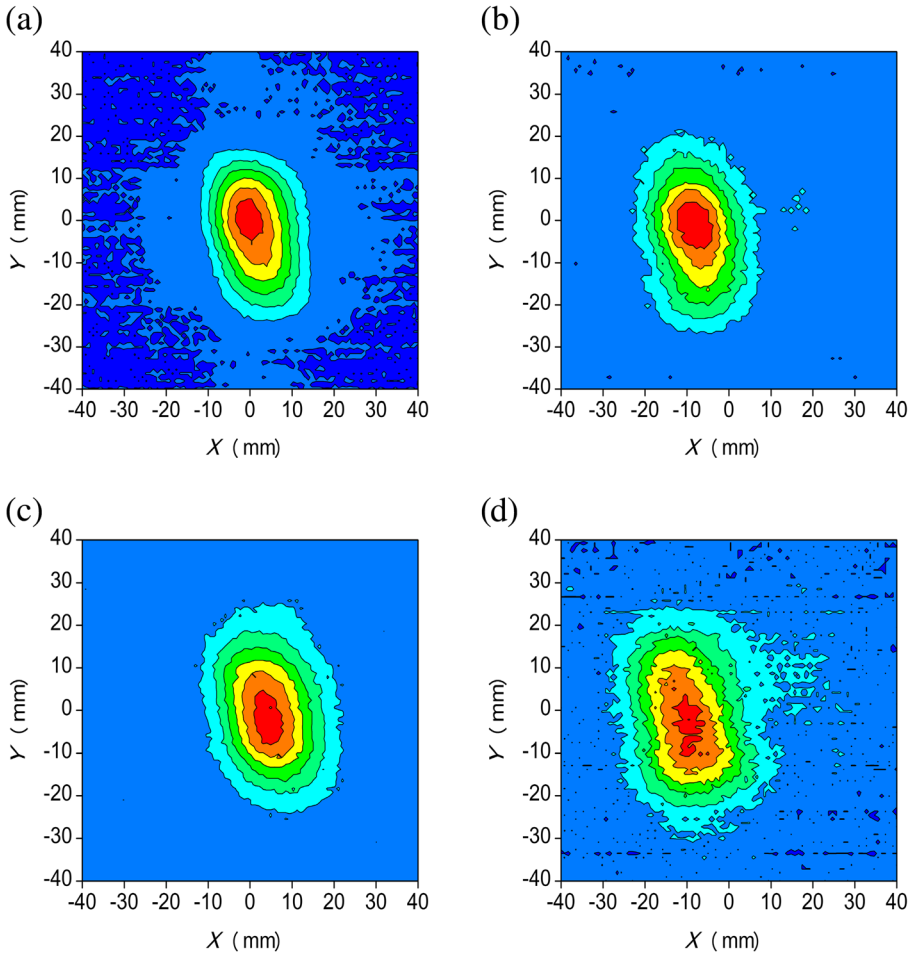
(a)

(b)

(c)

(d)

Fig. 9 Radiation patterns measured using an infrared camera with **a** $B=9.670$ T, **b** $B=8.840$ T, **c** $B=8.208$ T, and **d** $B=6.970$ T

of the double disks. These results are indicated by the closed circles, and they exceed 1 kW (10 % efficiency) for almost all cavity modes. For 265 GHz ($TE_{10,6}$ mode), the power measurements were not carried out using the double-disk window because the transmittance when using the single-disk window was high enough. At 202 GHz ($TE_{7,5}$ mode), no power improvement due to use of the double-disk window was observed, although the reason for this was unknown. The ratios of the powers are plotted in Fig. 11, where the horizontal axis indicates the calculated transmittance for a single-disk window. When the transmittance in the case of the double-disk window is nearly unity, then the power ratio P_1/P_2 represents the transmittance in the single-disk case. Here, P_1 and P_2 are the measured powers for the single- and double-disk windows. Therefore, if the data points lie around a straight line with an inclination of unity, then the measured transmittance matches the theoretical value well. Figure 11 shows that there is good agreement between the theoretical and experimental results, except for a few modes. The output power of the
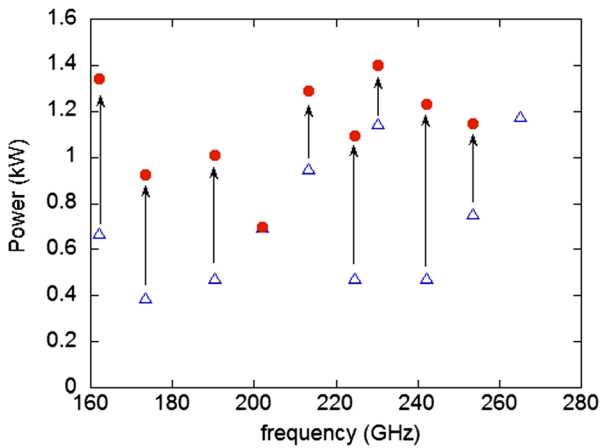
Fig. 10 Measured power with single-disk window (*open triangles*) and with double-disk window (*closed circles*)

modes other than the main mode improved and became comparable to that of the main mode when using the double-disk window.

4 Summary

The multifrequency Gyrotron FU CW GV has been developed. This gyrotron realizes step-like frequency variation almost every 10 GHz in the range from 162 to 265 GHz. The modes with almost identical radii of the caustic surface were chosen as the oscillation modes. Gaussian beam radiation was confirmed for these modes. The drop in the window transmittance because of its frequency dependence can be improved by introduction of a double-disk window, with which the output power of the expected mode oscillation exceeds 1 kW for almost all modes.
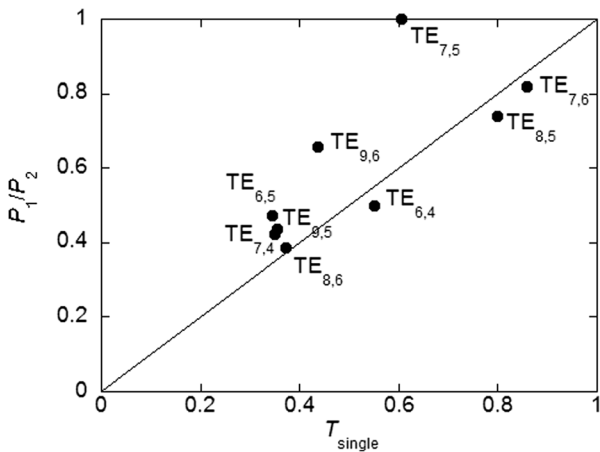

Fig. 11 Ratios of power values measured with the single-disk window, P_1, and with the double-disk window, P_2, plotted as a function of the calculated power transmittance

References

1. T. Idehara, I. Ogawa, S. Mitsudo, M. Pereyaslaverts, N. Nishida, K. Yoshida, IEEE Trans. Plasma Sci. 27, 340 (1999).
2. T. Saito, T. Nakano, H. Hoshizuki, K. Sakai, Y. Tatematsu, S. Mitsudo, I. Ogawa, T. Idehara, V. E. Zapevalov, Int. J. Infrared Milli. Waves 28, 1063 (2007).
3. V. Bratman, M. Glyavin, T. Idehara, Y. Kalynov, A. Luchinin, V. Manuilov, S. Mitsudo, I. Ogawa, T. Saito, Y. Tatematsu, V. Zapevalov, IEEE Trans. Plasma Sci. 37, 36 (2009).
4. T. Idehara, S.P. Sabchevski, J. Infrared Milli. Terahz. Waves 33, 667 (2012).
5. Y. Tatematsu, Y. Yamaguchi, T. Idehara, T. Ozeki, R. Ikeda, T. Kanemaki, I. Ogawa, T. Saito, J. Infrared Milli. Terahz Waves 33, 292 (2012).
6. Y. Tatematsu, Y. Yamaguchi, T. Idehara, T. Kawase, R. Ichioka, I. Ogawa, T. Saito, T. Fujiwara, J. Infrared Milli. Terahz Waves 35, 169 (2014).
7. Y. Tatematsu, Y. Yamaguchi, T. Idehara, T. Kawase, I. Ogawa, T. Saito, T. Fujiwara, J. Infrared Milli. Terahz Waves 35, 517 (2014).
8. Y. Tatematsu, Y. Yamaguchi, T. Kawase, R. Ichioka, I. Ogawa, T. Saito, T. Idehara, Phys. Plasmas 21, 083113 (2014).
9. T. Idehara, Y. Tatematsu, Y. Yamaguchi, E. M. Khutoryan, A. N. Kuleshov, K. Ueda, Y. Matsuki, T. Fujiwara, J. Infrared Milli. Terahz Waves 36, in press (2015). (doi 10.1007/s10762-015-0150-z).
10. Y. Matsuki, K. Ueda, T. Idehara, R. Ikeda, K. Kosuge, I. Ogawa, S. Nakamura, M. Toda, T. Anai, T. Fujiwara, J. Infrared Milli. Terahz Waves 33, 745 (2012).
11. F. Horii, T. Idehara, Y. Fujii, I. Ogawa, A. Horii, G. Entzminger, F. D. Doty, J. Infrared Milli. Terahz Waves 33, 756 (2012).
12. T. Yamazaki, A. Miyazaki, T. Suehara, T. Namba, S. Asai, T. Kobayashi, H. Saito, I. Ogawa, T. Idehara, S. Sabchevski, Phys. Rev. Lett. 108, 253401 (2012).
13. A. Miyazaki, T. Yamazaki, T. Suehara, T. Namba, S. Asai, T. Kobayashi, H. Saito, T. Idehara, I. Ogawa, Y. Tatematsu, J. Infrared Milli. Terahz. Waves, 35, 91 (2014).
14. A. Miyazaki, T. Yamazaki, T. Suehara, T. Namba, S. Asai, T. Kobayashi, H. Saito, Y. Tatematsu, I. Ogawa, T. Idehara, Prog. Theor. Exp. Phys. 2015, 011C01 (2015).
15. S. Mitsudo, S. Inagaki, I. N. Sudiana, K. Kuwayama, J. Adv. Mat. Res. 789, 279 (2013).
16. I. N. Sudiana, R. Ito, S. Inagaki, K. Kuwayama, K. Sako, S. Mitsudo, J. Infrared Milli. Terahz Waves 34, 627 (2013).
17. K. E. Kreischer, R. J. Temkin, Phys. Rev. Lett. 59, 547 (1987).
18. K. D. Hong, G. F. Brand, T. Idehara, J. Appl. Phys. 74 5250 (1993)
19. O. Prinz, A. Arnold, G. Gantenbein, Y.-H Liu, M. Thumm, D. Wagner, IEEE Trans. Electron Devices 56, 828 (2009).
20. R. J. Temkin, Terahertz Sci. Tech. 7, 1 (2014).
21. X. Yang, D. Eagner, B. Piosezyk, K. Koppenberg, E. Borie, R. Heidinger, F. Leuterer, G. Dammertz, M. Thumm, Int. J. Infrared Milli. Waves 24, 619 (2003).
22. P. F. Goldsmith, Quasioptical Systems, Gaussian Beam Quasioptical Propagation and Applications, (IEEE Press 1998) pp.266-280.
23. A. Möbius and M. Thumm, Gyrotron Oscillators, Their Principles and Practice, ed. by C. J. Edgcombe (Taylor & Francis, London, 1993) pp. 179-222.
24. M. V. Kartikeyan, E. Borie, M. K. A. Thumm, Gyrotrons, High-Power Microwave and Millimeter Wave Technology (Springer, Berlin Heidelberg, 2004) pp.127-146.
25. Y. Tatematsu, T. Saito, J. Jpn. Soc. Infrared Sci. Technol. 23, 93 (2013)
    (**in Japanese**).
26. Y. Yamaguchi, Y. Tatematsu, T. Saito, R. Ikeda, I. Ogawa, T. Idehara, in "Extended abstracts of 38th IRMM W-THz" (2013) Mo P1-54.
27. M. Thumm, State-of-the-art of high power gyro-devices and free electron masers, Update 2010, KIT Scientific Report 7575, KIT Scientific Publication, Karlsruhe, Germany, 2011.